Electronic structure and lattice dynamics of the magnetic shape-memory alloy Co_2NiGa

M. Siewert,[1] M. E. Gruner,[1] A. Dannenberg,[1] A. Hucht,[1] S. M. Shapiro,[2] G. Xu,[2] D. L. Schlagel,[3] T. A. Lograsso,[3] and P. Entel[1]

[1]*Faculty of Physics and Center for Nanointegration, CeNIDE, University of Duisburg–Essen, D-47048 Duisburg, Germany*

[2]*Condensed Matter Physics and Materials Science Department, Brookhaven National Laboratory, Upton, New York 11973, USA*

[3]*Ames Laboratory and Materials Science and Engineering, Iowa State University, Ames, Iowa 50011, USA*

(Received 31 March 2010; revised manuscript received 4 June 2010; published 20 August 2010)

In addition to the prototypical Ni-Mn-based Heusler alloys, the Co-Ni-Ga systems have recently been suggested as another prospective materials class for magnetic shape-memory applications. We provide a characterization of the dynamical properties of this material and their relation to the electronic structure within a combined experimental and theoretical approach. This relies on inelastic neutron scattering to obtain the phonon dispersion while first-principles calculations provide the link between dynamical properties and electronic structure. In contrast to Ni_2MnGa, where the softening of the TA_2 phonon branch is related to Fermi-surface nesting, our results reveal that the respective anomalies are absent in Co-Ni-Ga, in the phonon dispersions as well as in the electronic structure.

DOI: 10.1103/PhysRevB.82.064420 PACS number(s): 63.20.kd, 81.30.Kf, 61.66.Dk, 75.50.Cc

I. INTRODUCTION

Since the discovery of the giant magnetostriction or large magnetic field-induced strain in Ni_2MnGa,[1] which has meanwhile augmented to 10%, induced by reordering of martensitic twin variants under the action of an external magnetic field,[2] there is large interest in developing new magnetic shape-memory alloys (MSMA), for example, FePd, Fe_3Pt, $Ni_2Mn(Al,In,Sn,Sb)$, Ni_2FeGa, and $Co_2Ni(Al,Ga)$. The use of Ni_2MnGa in MSM devices is partially hindered by its low martensitic transformation temperature, bad ductility in the polycrystalline state, and low blocking stress level.[3] The common approach to improve the martensitic transformation temperature is to replace Ga by excess Mn, which favorably increases the valence-electron density. As a side effect, however, antiferromagnetic exchange interactions may be induced between nearest-neighbor Mn atoms, which do not improve the magnetic properties. Antiferromagnetic tendencies have been found for Ni-Mn-In, Ni-Mn-Sn, and Ni-Mn-Sb,[4,5] and also in Ni-Mn-Ga alloys.[6] In the latter case, a Slater-Pauling curve was derived showing the crossover from ferromagnetism to antiferromagnetism. Therefore, the primary interest of research is focusing on alloys with higher operation temperatures and better elastic properties compared to Ni_2MnGa. The binary Fe-based systems have too low martensite transformation temperatures and components as Pd may be too costly for mass production.

To overcome these problems, Wuttig and others suggested to intensely search for alternatives to Mn, focusing on Co-based MSMA.[7–9] Promising candidates for a thermoelastic transformation in the ferromagnetic state are $Co_2Ni(Al,Ga)$. In these materials the Mn atoms have been replaced by Ni to circumvent the problems arising from antiferromagnetic interactions in the material. Additionally, the original Ni atoms are replaced by Co in this system to introduce an element with a large magnetic moment securing a sufficiently high Curie temperature. Adding to their feasibility is better ductility in those alloys which can be traced back to a secondary γ phase,[10] a large transformation range,[11] and a high Curie temperature. The shape-memory effect has been investigated in a series of papers, see, for example, Ref. 12 and recent studies show excellent superelasticity.[13] This means that $Co_2Ni(Al,Ga)$ may be a promising MSMA.[14]

In austenite Ni_2MnGa, which has a $L2_1$-Heusler-type structure, the structural instability is often linked with an anomalous phonon softening of the transversal acoustic TA_2 branch in [110] direction.[15–18] The softening occurs at a fractional wave vector of $\xi=0.3-0.4$ depending upon the composition and becomes more prominent with decreasing temperature, approaching the martensitic transformation, and was frequently interpreted as precursor of the martensitic transformation. Similar anomalies can also be found in conventional shape-memory materials[19,20] and have been related to nesting parts of the Fermi surface in combination with strong electron-phonon coupling. The situation appears similar in Ni_2MnGa, where respective features have been identified in both channels of the electronic structure, in the minority bands[21] as well as in the majority bands.[22]

In this paper we focus our interest on the structural, vibrational, magnetic, and electronic differences between Ni_2MnGa and the $Co_2Ni(Al,Ga)$ alloys, although, we concentrate mostly on the Co-Ni-Ga alloy system. The difference in equilibrium reactions between Co-Ni-Al (eutectic reaction) and Co-Ni-Ga (peritectic reaction) (Ref. 10) leading to different microstructures is also important regarding the effectiveness of the shape-memory effect but this issue cannot be discussed in the frame of our *ab initio* investigations. Therefore, we mainly address the difference between Ni-Mn-Ga and Co-Ni-Ga alloys with respect to Fermi-surface nesting, dynamical, and magnetic properties. Since Ni_2MnGa is known to show pronounced Fermi-surface nesting behavior and large phonon softening,[18,23,24] the question arises whether in the Mn-free alloy system Co-Ni-Ga similar mechanisms are effective. In this context, we present first measurements of the [110] TA_2 phonons in $Co_{48}Ni_{22}Ga_{30}$ by means of inelastic neutron scattering. The results are related to first-principles calculations of the electronic structure, including Fermi surfaces as well as the full phonon dispersion of stoichiometric Co_2NiGa within the framework of density-

functional theory (DFT). We estimate the differences to the respective off-stoichiometric composition in terms of a rigid-band description and by considering supercells.

II. EXPERIMENTAL AND THEORETICAL DETAILS

The crystal of Co_2NiGa was grown at the Ames Laboratory, US DOE. The appropriate quantities of the elements (purity >99.99%) were cleaned and arc-melted several times under an argon atmosphere. The buttons were drop cast into a copper chill cast mold to ensure compositional homogeneity throughout the ingot. Crystal growth was done by the modified Bridgman technique in a resistance furnace. The as-cast ingot was placed in an alumina crucible and initially heated under a vacuum to 900 °C and then the furnace was backfilled with ultrahigh-purity argon to a pressure of 2.8×10^5 Pa to minimize evaporative losses. Following pressurization, heating was continued until the ingot reached a temperature of 1400 °C, held for 1 h before being withdrawn from the heat zone at a rate of 20 mm/h.

The size of the sample used in the neutron experiment was approximately $20 \times 4 \times 3$ mm^3 and was slightly off stoichiometry with an excess of $Ga:Co_{48}Ni_{22}Ga_{30}$ ($Co_{1.92}Ni_{0.88}Ga_{1.2}$). There were multiple grains in the sample separated by several degrees as observed in rocking curves. We were able to isolate one grain (mosaic ~0.5°) and observed the set of Bragg peaks associated with this grain, which we oriented with [001] perpendicular to the scattering plane. The measurements were performed about the (2,2,0) Brillouin zone along the transverse $[\zeta\text{-}\bar{\zeta}0]$ direction, which allows the measurement of the [110]-TA_2 phonons. Monitoring the intensity dependence of the spectra as a function of momentum q confirmed that the measured phonon peaks all originate from the same grain. The transition temperatures were determined by monitoring the (2,2,0) Bragg peak as a function of temperature. The M_s, M_f, A_s, A_f temperatures were 284.1 K, 269.4 K, 280.8 K, 295.2 K, respectively, which are in reasonable agreement with other samples of similar composition.[25] The transition was spread over 15 K and the hysteresis was about 11 K.

The neutron-scattering measurements were performed on the BT9 beam port at NIST research reactor. The spectrometer was operated in fixed final energy, $E_F = 14.7$ meV using pyrolytic graphite (PG) as monochromator and analyzer, and collimation of 40-20-20-40 throughout the instrument. A PG filter was placed after the analyzer to eliminate higher-order reflections of the analyzer.

The measurements were complemented by *ab initio* calculations of electronic, structural, and dynamic properties of stoichiometric and off-stoichiometric Co_2NiGa, which were obtained by means of DFT. For this purpose, we employed the Vienna *ab initio* simulation package (VASP) (Refs. 26 and 27) in combination with the projector augmented wave (PAW) method[28] and the generalized gradient approximation for the exchange-correlation functional in the formulation of Perdew, Burke, and Ernzerhof.[29] The employed PAW potentials explicitly included the semicore $3p^6$ electrons of Ni and the $3d^{10}$ electrons of Ga. The VASP code describes the Kohn-Sham orbitals using a plane-wave basis set, for which we use an energy cutoff of 460 eV. Off-stoichiometric compositions were modeled on the basis of a 16 atom supercell including optimization of the atomic positions using a conjugate-gradient algorithm in order to account for rearrangements induced by the larger Ga atoms. Brillouin-zone integration was carried out using a finite temperature smearing method with a smearing parameter $\sigma = 0.1$ eV and a Monkhorst-Pack grid of $15 \times 15 \times 15$ k points and $8 \times 8 \times 8$ k points in the full Brillouin zone for the four atom primitive cell and the 16 atom supercells, respectively. Energies were converged down to 10 μeV and forces down to 10 meV/Å. The k-mesh convergence was checked to guarantee an accuracy of better than 0.5 meV/atom for all tetragonal configurations. The Fermi surfaces were calculated on a mesh containing $39 \times 39 \times 39$ k points. For obtaining the electronic properties, the Brillouin-zone integration was carried out on the basis of the tetrahedron method with Blöchl corrections.

The phonon dispersions were obtained by means of the direct approach,[30–32] which uses the forces acting on the atoms of the supercell after applying individual nonequivalent displacements of atoms of the primitive cell, which allows the calculation of the dynamical matrix. Displacements and dynamical matrix were obtained with Dario Alfè's PHON package.[33] The size of the displacements was chosen to be 0.02 Å and supercell sizes of $4 \times 4 \times 4$ primitive cells in connection with a $2 \times 2 \times 2$ k mesh in the case of the stoichiometric composition were used. For off-stoichiometric compositions the original supercells containing 16 atoms were repeated two times in each direction and a $4 \times 4 \times 4$ k mesh was used.

Here, one should note that it has been pointed out previously that the fine details of the total-energy curves of prototype Ni_2MnGa depend, especially for the region with $c/a < 1$, whether a full-potential method has been used as well as on the magnitude of the finite temperature broadening employed in the Brillouin-zone integration.[9,34] We therefore carried out additional test calculations which revealed that the energy difference between $c/a = 1$ and $c/a = 1.4$ changes less than 1 meV/atom when using Methfessel-Paxton smearing with $\sigma = 0.1$ eV compared to the tetrahedron method with Blöchl corrections for the $L2_1$ structure of Co_2NiGa.

III. RESULTS

A. Martensitic transformations and binding surface in stoichiometric and off-stoichiometric Co-Ni-Ga

Before discussing the dynamical aspects of Co-Ni-Ga MSM alloys, it is important to recall the central features of the rich phase diagram shown in Fig. 1. The extrapolation of the stability regions of bcc-type B2 phases of the binary Co-Ga and Ni-Ga alloys suggests that ternary compositions with a bcc lattice structure, which may transform martensitically, might exist in the vicinity of the stoichiometric composition.[36] Experimental characterization reveals, however, that in order to obtain pure β (bcc) phases a Ga content of at least 30% is required, while at the stoichiometric composition a rather mixture of segregated β and γ (fcc) phases is found. This narrows the range of martensitically transforming compositions since with increasing Ga content (and

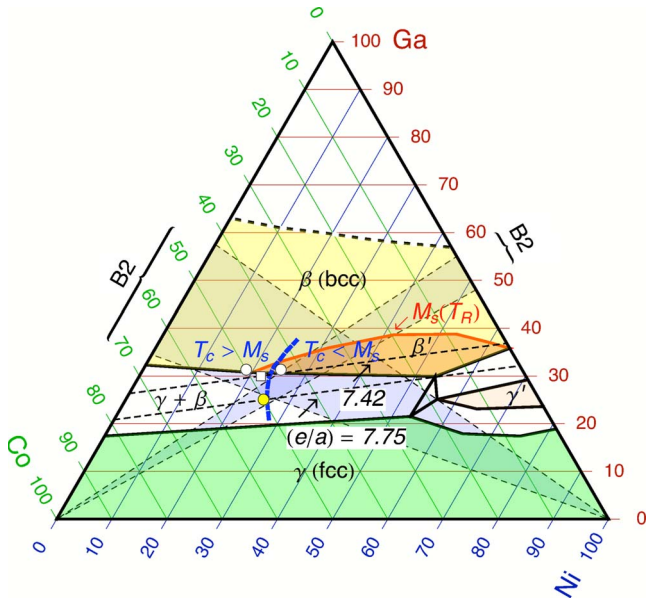

FIG. 1. (Color online) The Ga-Co-Ni phase diagram showing the martensitic phase at room temperature with the isothermal room-temperature martensite start temperature $M_s(T_R)$ represented in the isothermal section of 1000 °C, constructed from the data in Ref. 35. The isothermal section shows the equilibrium fcc- and bcc-like phases, γ (A1), γ' ($L1_2$), and β (B2), respectively, as well as the two-phase field $\gamma+\beta$ region. Tetragonal β' ($L1_0$) corresponds to the martensitic structure. The extrapolated B2 phases (dashed triangles) show the favorable overlapping β regions at 0 °C for the formation of magnetic-shape-memory (MSM) $L2_1$-like Heusler structures (Ref. 36). The yellow dot marks the perfect $L2_1$ Co_2NiGa compound on the dashed line of constant $e/a=7.75$. The second dashed line of constant $e/a=7.42$ goes through the white square corresponding to completely disordered β-phase $Co_{48}Ni_{22}Ga_{30}$ ($Co_{1.92}Ni_{0.88}Ga_{1.2}$) for which the phonon dispersions were measured by neutron-scattering experiment at room temperature. First-principles phonon calculations were done for $L2_1$ Co_2NiGa, $Co_8Ni_3Ga_5$ ($Co_2Ni_{0.75}Ga_{1.25}$), and $Co_7Ni_4Ga_5$ ($Co_{1.75}NiGa_{1.25}$), the latter are represented by white circles. The regions with Curie temperatures T_c larger or smaller than the martensite transformation temperatures M_s are separated by the thick blue line (constructed from the data in Ref. 11).

thus decreasing e/a), the martensitic transformation temperatures decrease. A similar behavior is obtained if Ni is replaced by Co. As a limit for nonvanishing martensite transition temperatures $e/a \approx 7.3$ has been proposed in the past.[36] On the other hand, the Curie temperatures show the opposite trend with increasing Co content, which means that a sufficient amount of Co is necessary to stabilize the ferromagnetism at appropriate operating temperatures. This dramatically narrows the range of compositions in which alloys with suitable MSM properties can be found.

Apart from the composition, the distribution of the atoms on the sublattices can play an important role for phase stability. While first studies considered a $L2_1$ full Heusler ordering as observed for Ni_2MnGa, later experimental studies reported Co-Ni-Ga alloys with a disordered B2 structure. The B2 structure consists of two interpenetrating disordered sublattices, which are occupied with different elemental ratios. This may delicately depend on the preparation conditions, which vary in order to avoid β-γ phase separation.

The theoretical approach used in our study does not facilitate the simulation of ideally disordered structures, as it requires the explicit modeling of disorder in large simulation cells. We therefore restrict the investigations to two paradigmatic distributions of atoms which can be realized in the primitive cell. This proves sufficient to disclose the essential physical trends. The first is the conventional $L2_1$ full Heusler structure. The body-centered lattice can be constructed by two interpenetrating rocksalt lattices, which are occupied alternating with Ni and Ga in the first case and completely by Co in the second. The alternative is the so-called inverse Heusler structure, which is experimentally observed, e.g., for Mn_2NiGa (see Refs. 37–39 for critical remarks),[37] the Fe_2CoAl compound[40] as well as for Fe_2CoGa,[41] and which has been predicted for a large number of different Heusler compounds in an extensive theoretical investigation by Gilleßen and Dronskowski.[42] In contrast to the full Heusler structure half of the Co atoms exchange their sites with the Ni atoms in this case which results in Co atoms becoming nearest neighbors.

Off-stoichiometric compounds with one excess Ga atom can be easily modeled using the 16 atom unit cell of the conventional and inverse Heusler structure as shown in Fig. 2. Our calculations suggest that all Ga atoms should be located on the same rocksalt lattice as the distribution of Ga over both sublattices generally results in higher-energy configurations. Thus it is straightforward to model off-stoichiometric compositions by as small as possible supercells obeying this condition. In order to keep the numerical effort tractable, we restricted the investigations to supercells consisting of 16 atoms, namely, $Co_8Ni_3Ga_5$ ($Co_2Ni_{0.75}Ga_{1.25}$) and $Co_7Ni_4Ga_5$ ($Co_{1.75}NiGa_{1.25}$), where Ga simply takes over the site of one of the respective elements on the same sublattice. As we intend to compare the binding surfaces of conventional and inverse Heusler structures of the same composition, we establish the respective compositions by analogous replacement of a Co/Ni atom on the other sublattice. The so-obtained two off-stoichiometric compositions in combination with the stoichiometric one encircle the experimental composition $Co_{48}Ni_{22}Ga_{30}$ ($Co_{1.92}Ni_{0.88}Ga_{1.2}$) as shown in Fig. 1.

The energy landscape as a function of the tetragonal distortion c/a is summarized in Fig. 3 for all three compositions. As the volume of the cells do not vary strongly upon tetragonal distortion, it is sufficient to calculate the energies for the respective equilibrium volume of the cubic phase ($c/a=1$), only. To ensure this, the equilibrium volumes for all tetragonal ($c/a \neq 1$) minima were determined in a second step. The respective volumes are listed in Table I in combination with the magnetic properties of the phases. The changes with respect to tetragonal distortion are typically small. For the alloys containing 50% Co, the inverse structure is energetically favored over the conventional full Heusler arrangement for the entire c/a range, while for the Co-depleted $Co_7Ni_4Ga_5$ supercell, the Heusler structure becomes energetically favored in the vicinity of the cubic phase ($c/a=1$). However, for the cubic phase the energy difference between both realizations of the Heusler structure is rather

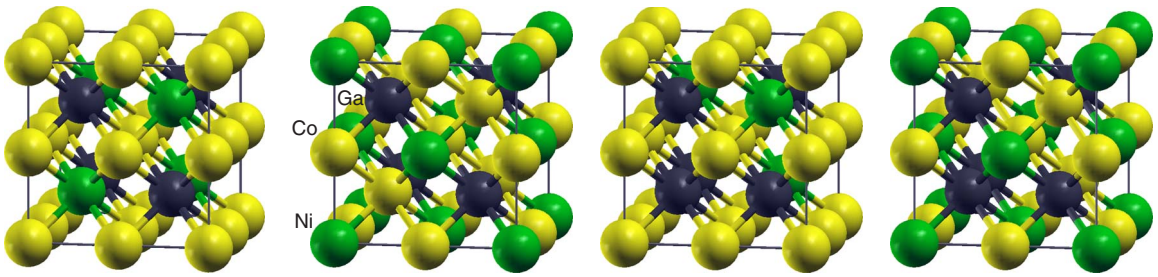

FIG. 2. (Color online) Schematic view of the (a) conventional Heusler structure ($L2_1$) with the Co atoms (bright yellow) occupying the corners, center, and faces of the simulation cell while the Ga atoms (black) and Ni atoms (medium green) occupy the other rocksalt sublattice and (b) the inverse structure of the stoichiometric composition. Some of the supercells with Ga excess are also plotted. The cell in (c) belongs to the Heusler structure of $Co_8Ni_3Ga_5$ ($Co_2Ni_{0.75}Ga_{1.25}$) where one Ni atom of the stoichiometric compound has been replaced by Ga. The cell in (d) belongs to the inverse Heusler structure of the $Co_7Ni_4Ga_8$ ($Co_{1.75}NiGa_{1.25}$) compound where one Co atom has been replaced by Ga.

small in all three cases, i.e., 14.62 meV/f.u. for Co_2NiGa, 14.6 meV/f.u. for $Co_{1.75}NiGa_{1.25}$, and 15.43 meV/f.u. for $Co_2Ni_{0.75}Ga_{1.25}$ which corresponds to temperatures on the order of 100 K. This is a strong indication that a disordered structure should be expected in a realistic experimental setup, rather than a competition between the two ordering cases. The binding curve representing the experimental systems might thus be seen as a superposition of the theoretical cases, which are discussed below in detail.

There are characteristic differences between the inverse and conventional Heusler structures appearing for all three compositions, which include even qualitative discrepancies between the conventional and inverse Heusler structure concerning the predicted ground states. These refer to the tetragonal distortion related to the absolute minimum of the binding curve observed for $c/a>1$, which is generally 100 meV lower in energy for the inverse compared to the conventional Heusler structure. In the case of $Co_8Ni_3Ga_5$ ($Co_2Ni_{0.75}Ga_{1.25}$) we even find a region of stability for the cubic structure for the full Heusler case (only a saddle point is found at $c/a=1.25$) as well as a well-defined minimum at $c/a=1.25$ for the inverse case while for $Co_7Ni_4Ga_5$ ($Co_{1.75}NiGa_{1.25}$) the full Heusler binding curve is nearly flat over a large range of tetragonal distortions. For the stoichiometric case, both representations show a global minimum for $c/a>1$. The optimum tetragonal distortion differs, however, significantly: $c/a=1.25$ for the inverse vs $c/a=1.41$ for the conventional structure, which results in a near-perfect fcc coordination. For the face-centered γ phase a Pt_2FeCu-type ordering has been proposed previously.[43] From our calculations, however, it appears that this ordering is by 137 meV/f.u. higher in energy than the two considered Heusler arrangements and thus is not further considered, here.

The general trend in experiment, increasing transformation temperature with increasing e/a, which can be expected to show up in a corresponding decrease in the energy of the tetragonal phase with respect to the cubic one, is well met by the six configurations investigated here. The conventional Heusler structures are furthermore characterized by slightly smaller equilibrium volumes than the inverse structures, which goes hand in hand with a significantly increased magnetic moment in the latter case. Another striking feature is the appearance of a second local minimum in the binding curve for $c/a<1$. Indeed, tetragonal or orthorhombic martensitic structures with $c/a\approx0.86$ have been reported in the literature for corresponding compositions.[11,44] However, structures with $c/a>1$ have also been reported for a body-centered-tetragonal structure as well as for the $L1_0$ structure.[45] This suggests an analogy to the prototypical MSM system Ni_2MnGa. Here the ground state is also predicted to be a nonmodulated structure with $c/a=1.25$ (which is found experimentally for off-stoichiometric compositions),[9,46–49] but the martensitic phase showing the desired MFIS is usually characterized by a modulated structure which is often described as a pseudotetragonal or orthorhombic structure with $c/a=0.9,\ldots,0.94$.[34]

As already discussed, the occurrence of modulated phases in Ni_2MnGa has been seen in relation to the anomalous temperature-dependent softening of the TA_2 mode in the vicinity of the premartensitic transition. This in turn was traced back to nesting features of the Fermi surface which can be connected with the same wave vector also describing the

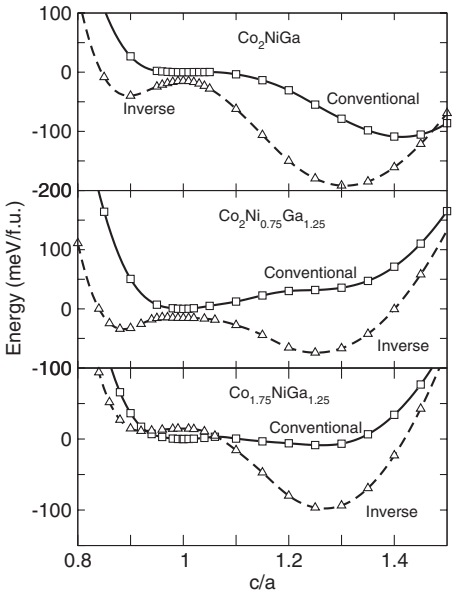

FIG. 3. Total-energy dependence under the variation in c/a from *ab initio* calculations for different compositions and conventional ($L2_1$ like) and inverse crystal structures.

TABLE I. Properties of the cubic structures and all energetic minima found in the total-energy curves of the investigated compounds. $\Delta E_{c/a}=E(c/a)-E(c/a=1)$ denotes the energy difference per formula unit between the minima and the cubic structure of the same system. The volume V, the bulk modulus B, and the magnetic moment M are also plotted.

System		e/a	c/a	$\Delta E_{c/a}$ (meV/f.u.)	V (Å^3/atom)	B (GPa)	M (μ_B/f.u.)
Co_2NiGa	Conventional	7.75	1.0		11.54	181	2.67
			1.41	109.2	11.57	180	2.92
	Inverse		0.9	25.18	11.63	178	2.83
			1.0		11.65	176	3.05
			1.31	177.1	11.55	181	2.76
$Co_2Ni_{0.75}Ga_{1.25}$	Conventional	7.31	1.0		11.67	180	2.15
	Inverse		0.88	18.71	11.78	171	2.49
			1.0		11.82	172	2.79
			1.25	60.2	11.73	175	2.29
$Co_{1.75}NiGa_{1.25}$	Conventional	7.38	1.0		11.72	173	2.11
			1.26	8.92	11.69	176	1.86
	Inverse		0.92	3.3	11.81	171	2.3
			1.0		11.83	174	2.49
			1.27	113.8	11.74	175	2.07

phonon anomaly. Primary aim of this paper is therefore to compare the phonon dispersion obtained in experiment for the true MSM composition with the theoretically calculated ones for the paradigmatic structures discussed above. This will allow us to explore, in how far the analogy to Ni_2MnGa is useful to explain the shape-memory features found in the Co-Ni-Ga system.

B. Phonon-dispersion relations

Neutron-scattering measurements were carried out to investigate the phonon dispersion with respect to the occurrence of phonon softening. The mode of interest is the [110]-TA_2 transverse mode propagating along the [110] direction corresponding to atomic displacements along the perpendicular $[1\bar{1}0]$ direction. It is this mode that exhibits anomalous behavior in nearly all bcc-based systems exhibiting martensitic phase transformation. Figure 4 shows the phonon-dispersion curve measured about the (2,2,0) Brillouin zone at three different temperatures. For comparison, the room-temperature measurements[16] of the isostructural compound Ni_2MnGa are also presented. It is clear that the dispersion curve behaves in a normal nearly sinusoidal way without any anomalies and it is not temperature dependent. This contrasts with the behavior in Ni_2MnGa where an anomaly occurs near $\mathbf{q_0}=(\frac{1}{3},\frac{1}{3},0)$ which becomes more pronounced as the transition temperature is approached. Although the depth and the position of the dip depends upon stoichiometry, all Ni_2MnGa samples show an anomaly along the TA_2 branch. Furthermore, in Ni_2MnGa a modulated structure is present with the appearance of diffuse scattering at $\mathbf{q_0}$, which becomes a Bragg peak in the premartensitic phase. Such excess diffuse scattering is also absent in Co_2NiGa.

Apart from neutron-scattering measurements, *ab initio* calculations provide a complementary approach to understand the dynamic properties of Co-Ni-Ga compounds. In Fig. 5, we compare the calculated phonon-dispersion curves of Ni_2MnGa and three of the paradigmatic Co-Ni-Ga structures discussed above. In agreement with the experimental data shown in Fig. 4, the stoichiometric full Heusler Co_2NiGa does not reveal an unstable phonon along the [110] direction which stands in contrast to the prototype MSMA Ni_2MnGa. Additionally the lower optical modes at the Γ point of Co_2NiGa move to considerably higher frequencies, thereby also losing the nearly perfect elemental character of

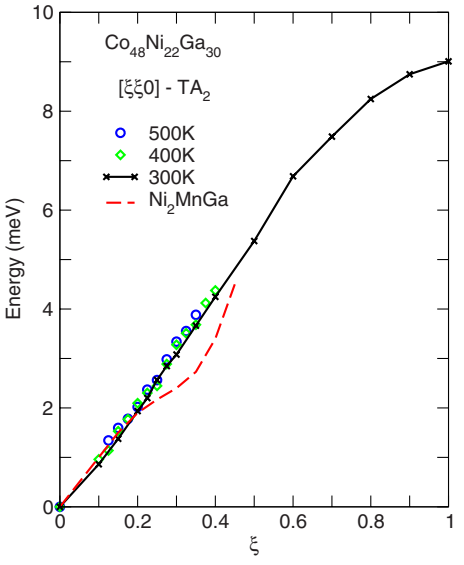

FIG. 4. (Color online) The measured dispersion curve of the [ξξ0]-TA_2 phonon branch in $Co_{1.92}Ni_{0.88}Ga_{1.2}$ at several temperatures. The data for stoichiometric Ni_2MnGa was taken from Ref. 16.

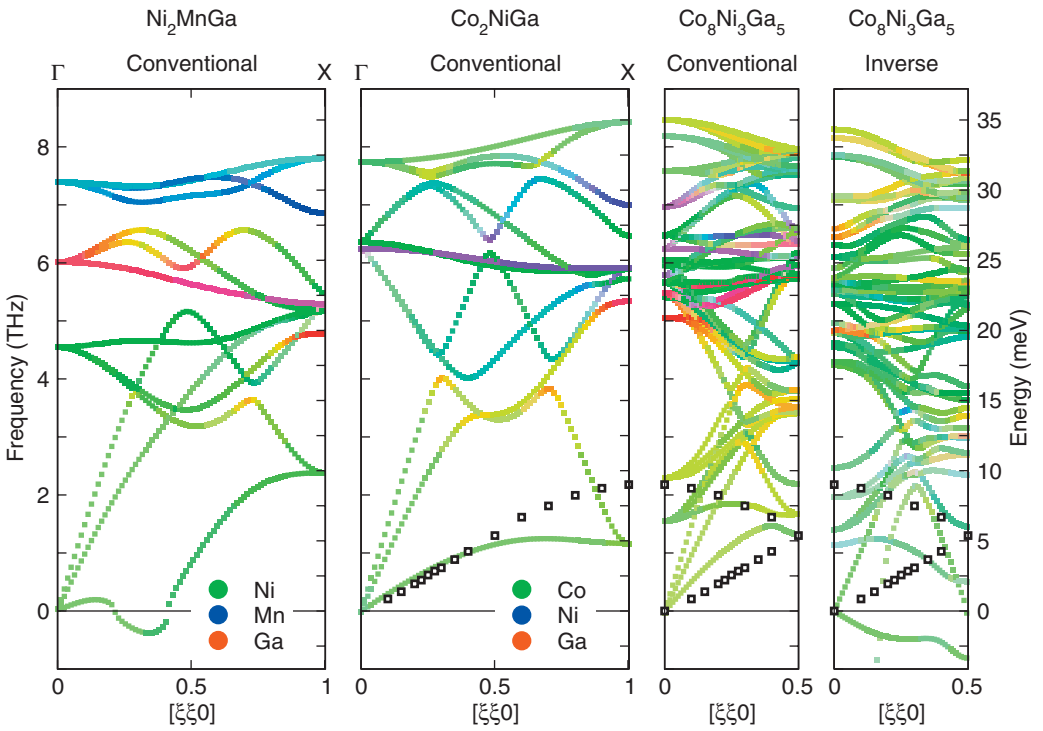

FIG. 5. (Color) Computed phonon-dispersion curves for the conventional Heusler structures of Ni_2MnGa, Co_2NiGa, and $Co_8Ni_3Ga_5$ ($Co_2Ni_{0.75}Ga_{1.25}$) and the inverse Heusler structure of $Co_8Ni_3Ga_5$ ($Co_2Ni_{0.75}Ga_{1.25}$) along the [110] direction. The contributions of the different elements are represented through a color scheme which is obtained from the eigenvectors belonging to the respective dynamical matrix. The squares denote the results of the measurements for the $Co_{48}Ni_{22}Ga_{30}$ ($Co_{1.92}Ni_{0.88}Ga_{1.2}$) sample.

the respective eigenmodes in Ni_2MnGa, as shown by the color coding in Fig. 5. Thus, in Co_2NiGa, the peculiar inversion of the Ga t_{2g} and Ni t_{2g} modes at the Γ point in Ni_2MnGa, which should be ordered according to their elemental masses, is also removed. The slope of the TA_2 branch of Co_2NiGa coincides well with the experiment up to halfway to the zone boundary. At the zone boundary the frequency of the TA_2 is significantly lower than in the measurements. It seems natural to trace this behavior back to the different valence-electron densities between the stoichiometric and the off-stoichiometric compositions, which lead to different shapes of the binding surface as shown in Fig. 3. We therefore calculated for comparison the phonon dispersion of the $Co_8Ni_3Ga_5$ ($Co_2Ni_{0.75}Ga_{1.25}$) full Heusler structure discussed above. Since the primitive cell now contains 16 atoms as opposed to four atoms in the case of Co_2NiGa with correspondingly larger extensions, the Brillouin zone becomes smaller, while the number of branches is increased accordingly. For the larger cell, the Brillouin zone extends now to half the wave vector of the original zone. To obtain the phonon dispersions in the original zone scheme, the appropriate branches extending in opposite direction from the zone boundary to the Γ point thus need to be unfolded. This is, of course, only perfectly possible for the stoichiometric case, where we also find according degeneracies. Instead, we rather fold the experimental data in order to allow a comparison. We find that in the nonstoichiometric case, the initial slope of the TA_2 branch is now considerably steeper. However, the second half of the experimental branch reaching the original zone (which is now folded back to the Γ point) coincides much better with the theory, where we find a bunch of branches with nearly coincident frequencies. The slightly brighter color reveals that the contribution from Ni atoms is lower compared to the stoichiometric case and a second group of branches arrives at Γ at significantly decreased frequencies. The change in the coloring along the q path indicates that branches from these two sets may be subject to an anticrossing, which may not be well resolved in the calculated plots due to the only twofold repetition of the unit cell used in the calculations.

In contrast to the conventional full Heusler alloys, all dispersions corresponding to the inverse structures exhibit imaginary frequencies. As an example, we present in Fig. 5 the dispersion in [110] direction of the inverse $Co_8Ni_3Ga_5$ ($Co_2Ni_{0.75}Ga_{1.25}$) alloy. The imaginary mode at the gamma point, which contains contributions from all atoms comes from the energetically unstable situation at $c/a=1$ which only has a saddle point in the binding curve in Fig. 3 with respect to tensile and compressive distortions. The bluish color of the low-lying (pseudo-)optical modes at the Γ point and the zone boundary reveals, that these modes, which are presumably pushing down the imaginary branches, are dominated by the Ni species. Thus placement of the Ni atoms in the Co sublattice can be made responsible for the occurrence of unstable modes in the inverse structure.

The calculation of the phonon-dispersion curves for the crystal structures of all three different compositions plotted in Fig. 3 revealed that the inverse Heusler structures, although being energetically favored show phonon softening up to imaginary frequencies. Thus, these structures are not

stable at low temperatures. In contrast to that the Heusler structures all have stable phonon dispersion curves in the cubic state. However, there are still quantitative disagreements between the measured and calculated dispersions. The origin of these differences can be related to disorder and the differences in composition.

While the inverse Heusler structures should be the ground state of all investigated compositions, it is reasonable that depending on the growth process of the crystal a disordered structure with coexisting properties of the Heusler as well as of the inverse structure is formed. One indication for this approach can be gained from the total-energy curves. The energy differences between different minima of the curves can give a first approximation to M_s. In the case of the inverse Heusler structures of the investigated Co-Ni-Ga compounds this would however mean that M_s is significantly above room temperature which is in contrast to the experiment. Also the fact that no phonon softening can be observed in the measurements is in agreement with the Heusler structure and cannot be explained through the *ab initio* results for the inverse structure. However, there are also experimental findings that are in good agreement with the calculated results of the inverse Heusler structure. First of all the calculated energy curves for the Heusler structures of $Co_2Ni_{0.75}Ga_{1.25}$ and $Co_{1.75}NiGa_{1.25}$ do not indicate that the systems undergo a martensitic transformation. While the global minimum of the Heusler structure of $Co_2Ni_{0.75}Ga_{1.25}$ can be found in the cubic $L2_1$ structure, a very flat, nearly degenerated energy curve can be observed in the case of $Co_{1.75}NiGa_{1.25}$. Thus, although a martensitic transformation can clearly be seen in the experiment, the ordered Heusler structure is not able to describe this behavior in the case of off-stoichiometric compounds. A second remarkable fact that is in disagreement with the findings for the ordered Heusler structure is that the *ab initio* results reveal no energetic minima for $c/a<1$.

In conclusion, our results suggest that the remaining differences between theory and experiment may rather be related to the partial disorder present in the experimental sample, which presumably contains Ni atoms on both, the Ga and the Co sublattices. It should be kept in mind that inverse and conventional Heusler structures are characterized by different atomic volumes and different magnetic states of the Co ions, which will probably result in significant atomic displacements of the atoms from their ideal lattice positions in the partially disordered alloy with B2 structure. This bears similarities to the situation in the Fe-based Invar and magnetic shape-memory materials, where considerable static displacements are also encountered.[50,51] In this case, for the ordered Fe_3Pt MSMA, a strong anomalous softening of the TA_1 branch in [110] direction is found at the zone boundary, which disappears in the disordered case in favor of a smeared out anomaly much closer to the Γ point.[52–55] Thus, the type and degree of disorder of a Co-Ni-Ga alloy, which is controlled experimentally by the annealing conditions, should be considered very important for the martensitic transformation and the (magnetic) shape-memory properties of the sample.

C. Electronic structure and Fermi surface of Co-Ni-Ga alloys

In the past, the martensitic instability in Ni_2MnGa has frequently been linked to nesting parts of the Fermi surface which can be connected by a wave vector corresponding to the instability of the TA_2 branch.[21,22] Although the phonon dispersions have already demonstrated that the situation is different for the Co-Ni-Ga system, a comparison of the corresponding Fermi surfaces may reveal further evidence. Figure 6 shows the Fermi surfaces of the spin-down channel of stoichiometric Ni_2MnGa and Co_2NiGa, as well as off-stoichiometric compositions, which are modeled by changing the band filling in the spirit of a simple rigid-band picture. The direct comparison of the Fermi surfaces of the stoichiometric compounds immediately reveals that the large flat portions of the Fermi surface present for Ni_2MnGa, which allegedly give rise to the Kohn anomaly, are largely reduced or absent for stoichiometric Co_2NiGa. Here, only the jungle-gym-type crossings close to the face center of the extended zone scheme remain but they appear expanded and additionally rounded. Upon reduction in the valence-electron concentration, also these remaining flat features disappear which is in accordance with the entirely stable phonon dispersion of $Co_8Ni_3Ga_5$ shown in Fig. 5. The inverse structures, which exhibits a strongly reduced Fermi surface for the stoichiometric case, also does not reveal the corresponding features. In this light, it appears natural to relate the absence of Fermi-surface nesting in the Co-based system to the absence of phonon softening, because the term which renormalizes the phonon frequencies due to the electron-phonon interaction consists of two factors, the electron-phonon matrix elements and the electric charge susceptibility $\chi_{00}(q)$ in each spin channel. The absence of Fermi-surface nesting reduces the latter factor. However, the electron-phonon matrix elements can still be large and can be the cause of the martensitic instability.

For the prototype MSMA Ni_2MnGa, the martensitic transformation is commonly interpreted in terms of a band Jahn-Teller effect, which is originating from a redistribution of Ni e_g states, which form a peak in the minority density of states (DOS) slightly below E_F.[9,49,56,57] This gives rise to the idea that a more detailed characterization of the structural transformation in Co-Ni-Ga can be obtained in an analogous way from an inspection of the electronic densities of states corresponding to the minima in the total-energy curves. A representative selection is shown in Figs. 7(a)–7(d). Because of the different valence-electron concentration of $e/a=7.75$ in case of Co_2NiGa compared to $e/a=7.5$ for Ni_2MnGa, the situation is however slightly different and stability considerations are more subtle. The tetragonal transformation in stoichiometric Co_2NiGa (Heusler structure) leads to a shift of the hump that can be found in the majority-spin channel just below E_F at $c/a=1$, shown in Fig. 7(a), to a position well above E_F at $c/a=1.41$, cf., Fig. 7(b). This leads indeed to an overall reduction in the number of states at E_F in the majority-spin channel. In the minority-spin channel, however, a pseudogap opens around E_F in the $L2_1$ phase while the number of states at the Fermi level is largely increased in the tetragonally distorted structure. This increase is again mainly driven by the Co states while all other partial contri-

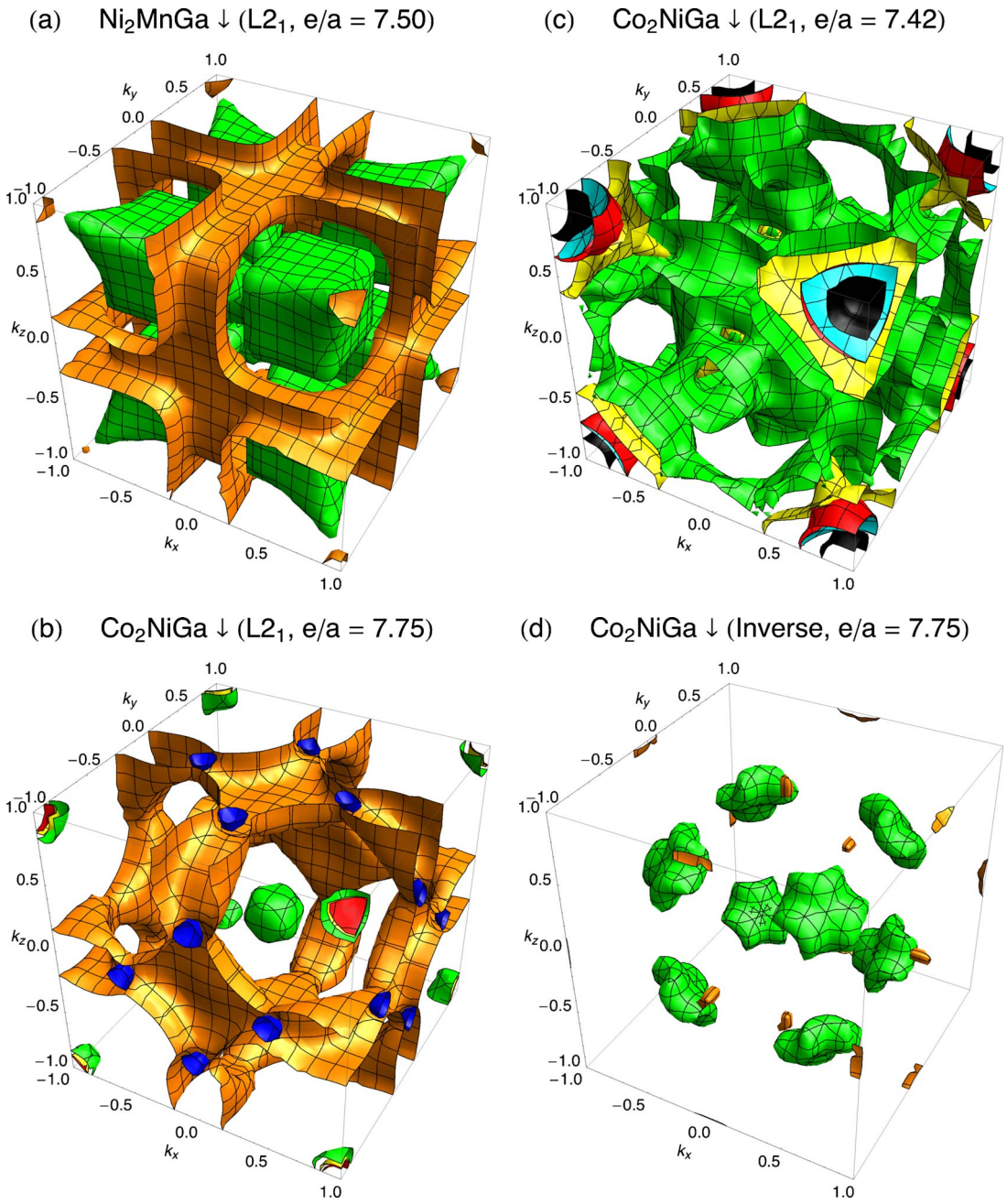

FIG. 6. (Color online) Fermi surfaces of (a) Ni_2MnGa (upper left, adapted from Ref. 24) and [(b)–(d)] Co_2NiGa for different valence-electron concentrations e/a in a repetitive scheme of the Brillouin zone. The Γ point can be found in the center of the displayed cubes as well as in each corner of the cubes. Different colors denote different bands crossing E_F. The Fermi surfaces of the Co-Ni-Ga systems all refer to the same color scheme. Here, only the Fermi surfaces corresponding to the minority-spin channels are plotted.

butions do not show any significant changes during the tetragonal transformation. The tetragonal distortion in Co_2NiGa is mainly stabilized by the shift in the spin-up channel and the broadening of the Ni pseudogap in the spin-down channel.

The change from the conventional to the inverse structure results in a complete reconstruction of the minority spin density of states in the vicinity of E_F, as can be seen from Fig. 7(c). In principle, the Fermi level is located in a region of increased DOS, which is interrupted by a deep and narrow gap right at E_F being responsible for the extremely small Fermi surface shown at the bottom right of Fig. 6. This rather narrow gap will easily fill up at finite temperatures, which will negatively affect the relative stability of the inverse structure. Another important aspect is that in the inverse case a Ni state concentrates in a peak right below E_F. This means that, in order to gain further insight concerning a possible electronic origin of the martensitic transformation, detailed calculations of the electronic structure of the alloys are necessary, which are entirely disordered with respect to the positions of the transition metal elements. This might be modeled in a more efficient way by means of the coherent-

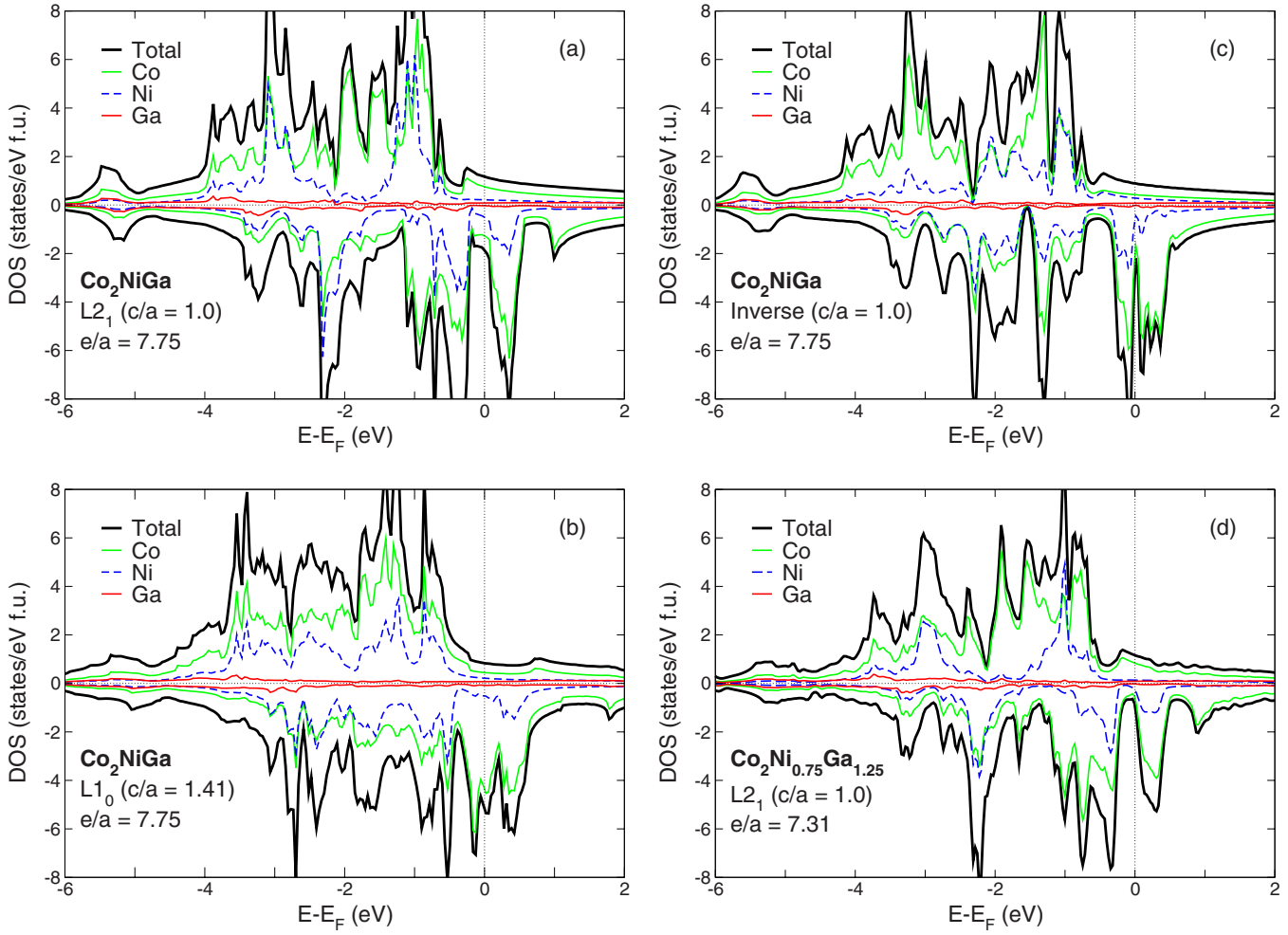

FIG. 7. (Color online) Partial and total densities of states of Co_2NiGa for the full Heusler structure at (a) $c/a=1$ and (b) $c/a=1.41$, (c) the inverse Heusler structure in the cubic state and (d) $Co_8Ni_3Ga_5$ ($Co_2Ni_{0.75}Ga_{1.25}$) in the full Heusler structure.

potential approximation than within the supercell approach used in the present study.

While the addition of Ga generally stabilizes the austenitic phase, changes in stoichiometry by Ga excess do not result in a qualitative change in the DOS, which is demonstrated in Fig. 7(d) at the example of the conventional Heusler structure of $Co_8Ni_3Ga_5$. Here, we observe that the number of transition-metal states is more or less continuously reduced over the whole energy range, rather than a mere shift of the Fermi level in a rigid-band fashion, which one might naively expect from the changed valence-electron concentration. A similar picture also holds for the tetragonally distorted case (not shown). The reduction in Co and Ni states in the pseudogap gap in the minority-spin channel close to E_F in Fig. 7(d) may, however, be a stabilizing factor for the cubic phase.

IV. CONCLUSIONS

Stoichiometric and off-stoichiometric Co-Ni-Ga compounds have been investigated by *ab initio* methods and compared to experimental measurements. We find that the calculated phonon-dispersion curves do not exhibit phonon softening in agreement with neutron-scattering experiments. The calculations of the binding energies for different compositions and crystal structures show that the $L2_1$ structure of stoichiometric Co_2NiGa is not energetically favored at low temperatures but rather a tetragonally distorted structure with $c/a=1.41$. We find that Ga excess increases the stability of the cubic structure in the conventional Heusler alloys and shifts the energy minimum of the martensitic phase toward smaller tetragonal distortions.

In contrast to Ni_2MnGa, we neither encounter extensive Fermi-surface nesting nor signatures of a band Jahn-Teller effect driving the martensitic transformation in the ordered cubic structure of Co_2NiGa as well as in the off-stoichiometric compositions. Our results point to a coexistence of the conventional Heusler and the inverse structures, which indicates that the experimentally realized structures are inherently disordered. Although phonon softening has not been observed in the measurements as well as in the calculations, a martensitic transformation can be found in the material. The differences between the experimental and theoretical results can be accounted to the fact that the effect of disorder cannot be taken into account in the calculations yet. Additionally the compositions that can be modeled by the

supercell approach still defer slightly from the composition of the experimental sample.

ACKNOWLEDGMENTS

Work at Ames and Brookhaven is supported by the U. S. Department of Energy under Contracts No. DE-AC02-7CH11358 and No. DE-AC02-76CH00016, respectively. Work in Duisburg is supported by Deutsche Forschungsgemeinschaft within the priority program SPP 1239. The calculations have been carried out on the parallel computing installations of the University Duisburg–Essen, Technical University Dortmund and Jülich Supercomputing Center.

[1] K. Ullakko, J. K. Huang, C. Kantner, R. C. O'Handley, and V. V. Kokorin, Appl. Phys. Lett. **69**, 1966 (1996).
[2] A. Sozinov, A. A. Likhachev, N. Lanska, and K. Ullakko, Appl. Phys. Lett. **80**, 1746 (2002).
[3] I. Karaman, H. E. Karaca, B. Basaran, D. C. Lagoudas, Y. I. Chumlyakov, and H. J. Maier, Scr. Mater. **55**, 403 (2006).
[4] S. Aksoy, M. Acet, P. P. Deen, L. Manosa, and A. Planes, Phys. Rev. B **79**, 212401 (2009).
[5] V. D. Buchelnikov, P. Entel, S. V. Taskaev, V. V. Sokolovsky, A. Hucht, M. Ogura, H. Akai, M. E. Gruner, and S. K. Nayak, Phys. Rev. B **78**, 184427 (2008).
[6] J. Enkovaara, O. Heczko, A. Ayuela, and R. M. Nieminen, Phys. Rev. B **67**, 212405 (2003).
[7] M. Wuttig, J. Li, and C. Craciunescu, Scr. Mater. **44**, 2393 (2001).
[8] K. Oikawa, T. Ota, F. Gejima, T. Ohmori, R. Kainuma, and K. Ishida, Mater. Trans. **42**, 2472 (2001).
[9] A. Ayuela, J. Enkovaara, K. Ullakko, and R. M. Nieminen, J. Phys.: Condens. Matter **11**, 2017 (1999).
[10] J. Liu and J. Li, Scr. Mater. **55**, 755 (2006).
[11] K. Oikawa, T. Ota, Y. Imano, T. Omori, R. Kainuma, and K. Ishida, J. Phase Equilib. Diffus. **27**, 75 (2006).
[12] M. Zhang, E. Bruck, F. De Boer, and G. Wu, J. Phys. D: Appl. Phys. **38**, 1361 (2005).
[13] X. F. Dai *et al.*, Appl. Phys. Lett. **87**, 112504 (2005).
[14] J. Dadda, H. Maier, I. Karaman, H. Karaca, and Y. Chumlyakov, Scr. Mater. **55**, 663 (2006).
[15] A. Zheludev, S. M. Shapiro, P. Wochner, A. Schwartz, M. Wall, and L. E. Tanner, Phys. Rev. B **51**, 11310 (1995).
[16] A. Zheludev, S. M. Shapiro, P. Wochner, and L. E. Tanner, Phys. Rev. B **54**, 15045 (1996).
[17] L. Mañosa, A. Planes, J. Zarestky, T. Lograsso, D. L. Schlagel, and C. Stassis, Phys. Rev. B **64**, 024305 (2001).
[18] A. T. Zayak, P. Entel, J. Enkovaara, A. Ayuela, and R. M. Nieminen, Phys. Rev. B **68**, 132402 (2003).
[19] X. Huang, I. I. Naumov, and K. M. Rabe, Phys. Rev. B **70**, 064301 (2004).
[20] G. L. Zhao and B. N. Harmon, Phys. Rev. B **48**, 2031 (1993).
[21] C. Bungaro, K. M. Rabe, and A. Dal Corso, Phys. Rev. B **68**, 134104 (2003).
[22] Y. Lee, J. Y. Rhee, and B. N. Harmon, Phys. Rev. B **66**, 054424 (2002).
[23] C. P. Opeil, B. Mihaila, R. K. Schulze, L. Mañosa, A. Planes, W. L. Hults, R. A. Fisher, P. S. Riseborough, P. B. Littlewood, J. L. Smith, and J. C. Lashley, Phys. Rev. Lett. **100**, 165703 (2008).
[24] P. Entel, V. D. Buchelnikov, M. E. Gruner, A. Hucht, V. V. Khovailo, S. K. Nayak, and A. T. Zayak, Mater. Sci. Forum **583**, 21 (2008).
[25] P. Brown, K. Ishida, R. Kainuma, T. Kanomata, K.-U. Neumann, K. Oikawa, B. Ouladdiaf, and K. Ziebeck, J. Phys.: Condens. Matter **17**, 1301 (2005).
[26] G. Kresse and J. Furthmüller, Phys. Rev. B **54**, 11169 (1996).
[27] G. Kresse and D. Joubert, Phys. Rev. B **59**, 1758 (1999).
[28] P. E. Blöchl, Phys. Rev. B **50**, 17953 (1994).
[29] J. P. Perdew, K. Burke, and M. Ernzerhof, Phys. Rev. Lett. **77**, 3865 (1996).
[30] G. Kresse, J. Furthmüller, and J. Hafner, Europhys. Lett. **32**, 729 (1995).
[31] X. Gonze and C. Lee, Phys. Rev. B **55**, 10355 (1997).
[32] K. Parlinski, Z. Q. Li, and Y. Kawazoe, Phys. Rev. Lett. **78**, 4063 (1997).
[33] D. Alfè, Comput. Phys. Commun. **180**, 2622 (2009).
[34] A. T. Zayak, P. Entel, J. Enkovaara, A. Ayuela, and R. M. Nieminen, J. Phys.: Condens. Matter **15**, 159 (2003).
[35] R. Ducher, R. Kainuma, and K. Ishida, J. Alloys Compd. **466**, 208 (2008).
[36] C. Craciunescu, Y. Kishi, T. Lograsso, and M. Wuttig, Scr. Mater. **47**, 285 (2002).
[37] G. D. Liu, X. F. Dai, S. Y. Yu, Z. Y. Zhu, J. L. Chen, G. H. Wu, H. Zhu, and J. Q. Xiao, Phys. Rev. B **74**, 054435 (2006).
[38] G. D. Liu, J. L. Chen, Z. H. Liu, X. F. Dai, G. H. Wu, B. Zhang, and X. X. Zhang, Appl. Phys. Lett. **87**, 262504 (2005).
[39] S. R. Barman and A. Chakrabarti, Phys. Rev. B **77**, 176401 (2008).
[40] A. K. Grover, R. G. Pillay, V. Nagarajan, and P. N. Tandon, J. Magn. Magn. Mater. **15-18**, 699 (1980).
[41] N. K. Jaggi, K. R. P. M. Rao, A. K. Grover, L. C. Gupta, R. Vijayaraghavan, and L. D. Khoi, Hyperfine Interact. **4**, 402 (1978).
[42] M. Gilleßen and R. Dronskowski, J. Comput. Chem. **31**, 612 (2010).
[43] X. Dai, G. Liu, Y. Li, J. Qu, J. Li, J. Chen, and G. Wu, J. Appl. Phys. **101**, 09N503 (2007).
[44] C. M. Craciunescu, Y. Kishi, M. De Graef, T. A. Lograsso, and M. Wuttig, Proc. SPIE **4699**, 235 (2002).
[45] S. Sarma and A. Srinivasan, Adv. Mater. Res. **52**, 103 (2008).
[46] V. V. Godlevsky and K. M. Rabe, Phys. Rev. B **63**, 134407 (2001).
[47] A. Zayak, W. A. Adeagbo, P. Entel, and V. D. Buchelnikov, Phase Transitions **78**, 259 (2005).
[48] P. Entel, V. D. Buchelnikov, V. V. Khovailo, A. T. Zayak, W. A. Adeagbo, M. E. Gruner, H. C. Herper, and E. F. Wassermann, J. Phys. D: Appl. Phys. **39**, 865 (2006).
[49] A. Ayuela, J. Enkovaara, and R. M. Nieminen, J. Phys.: Condens. Matter **14**, 5325 (2002).
[50] F. Liot and I. A. Abrikosov, Phys. Rev. B **79**, 014202 (2009).

[51] M. E. Gruner, Mater. Res. Soc. Symp. Proc. **1200E**, 1200 (2010).
[52] Y. Noda and Y. Endoh, J. Phys. Soc. Jpn. **57**, 4225 (1988).
[53] J. Kästner, W. Petry, S. Shapiro, A. Zheludev, J. Neuhaus, T. Roessel, E. Wassermann, and H. Bach, Eur. Phys. J. B **10**, 641 (1999).
[54] J. Kästner, J. Neuhaus, E. Wassermann, W. Petry, B. Hennion, and H. Bach, Eur. Phys. J. B **11**, 75 (1999).
[55] M. E. Gruner, W. A. Adeagbo, A. T. Zayak, A. Hucht, and P. Entel, Phys. Rev. B **81**, 064109 (2010).
[56] P. Brown, A. Y. Bargawi, J. Crangle, K.-U. Neumann, and K. Ziebeck, J. Phys.: Condens. Matter **11**, 4715 (1999).
[57] S. Fujii, S. Ishida, and S. Asano, J. Phys. Soc. Jpn. **58**, 3657 (1989).